

Hydrophilicity and Lipophilicity of Cellulose Crystal Surfaces

Oliver Biermann, Erich Hädicke,
Sebastian Koltzenburg, and Florian Müller-Plathe*

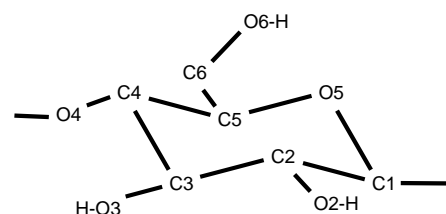
Cellulose is one of the most abundant biopolymers and a basis for many industrial derivatives and products. Its surface physics and chemistry are important for the understanding of adhesion to other materials (e.g. in nanocomposites of cellulose fiber reinforced thermoplastics),^[1] adsorption processes from solution (e.g. in paper production),^[2] and of industrial processes that start from a cellulose slurry (e.g. the preparation of cellulose derivatives, where often counter-intuitive substitution preferences are found).^[3] Although applications cover many areas of chemistry, biology and technology, the cellulose surface is still not well understood. The situation is complicated by the simultaneous presence of several phases in natural and processed cellulose fibers: There are three principal crystalline phases, triclinic (type I α) and monoclinic (type I β), and type II, with two likely surfaces each, as well as varying contents of amorphous material. Not even the behaviour of the crystalline surfaces towards water and hydrophobic organics has been fully characterized on a molecular level.

Molecular dynamics (MD) simulations with empirical force fields provide a detailed description of molecular systems. Provided the force field is realistic, the system is large enough to avoid finite-size effects, and the simulations last long enough to explore the relevant phase space, MD can deliver information complementary to experiments.^[4] We have undertaken MD simulations to better understand the cellulose surface. In particular, we attempt to characterize the cellulose in its behavior towards water (hydrophilicity/hydrophobicity) and towards apolar parts of organic molecules (lipophilicity/lipohobicity). We use simulation techniques that yield spatially resolved adsorption free energies for the respective moiety, to obtain charts of hydrophilicity and lipophilicity. While a comparative study of all possible cellulose surfaces would be desirable from a scientific and technological viewpoint, we have to restrict the simulations to the two surfaces of crystalline cellulose I β because of the computational cost.

Experimentally, the surface of crystalline cellulose has been visualized by atomic force microscopy (AFM). One important result is that it preserves the underlying crystal structure, as can be seen from unit cell parameters obtained by AFM, which compare well with those from X-ray diffraction.^[5–7] Computational studies have mainly investigated the bulk behavior of crystalline cellulose.^[8–12] The MD simulations of

Heiner and Teleman^[13, 14] explored the interface between triclinic (I α) and monoclinic (I β) cellulose and water.

We simulated the 110 (“wide”) and 1 $\bar{1}$ 0 (“narrow”) surfaces of monoclinic (I β) cellulose in contact with water. Except for the in-plane distance between parallel chains (0.614 (110), 0.540 nm (1 $\bar{1}$ 0), room temperature values corrected to 333 K using the experimental thermal expansion coefficient^[15]), they are very similar: The chains run parallel to the surface and the cellobiose units tilt out of the surface plane by about 45°. The cellulose was modelled as a slab of 6 \times 8 (deep \times wide) parallel chains of three cellobiose units each, cut from the crystal structure at the respective crystal face.^[16] In both cases, eight parallel chains run along the surface in the *x* direction. Neighboring chains are shifted along *x* by half an anhydroglucose unit (quarter of a cellobiose unit). The C6 groups point in the direction of the crystal and the water alternatingly (Scheme 1 shows the atomic numbering). The *z*



Scheme 1. Atom labeling in the anhydroglucose unit of cellulose.

direction is the surface normal, *z* = 0 being the point where the densities of water and cellulose are equal. Orthorhombic periodic boundary conditions were applied (this necessitated a small distortion of the unit cell by 1.2° with respect to the monoclinic crystal structure but gained substantial simulation speed). In the *z* direction, there is a gap between the upper surface of the cellulose slab and the nearest periodic image of its lower surface of 4.495 and 5.107 nm for the 110 and 1 $\bar{1}$ 0 surface, respectively; this gap is filled with 2197 water molecules. Three independent simulations were conducted for each surface. Each was equilibrated for about 1 ns and then sampled for about 1.0–1.3 ns with a time step of 0.002 ps. Coordinates were written out for analysis every 0.6 ps. The temperature *T* was maintained at 333 K using the Berendsen thermostat^[17] with a coupling time of 0.5 ps. We used the GROMOS96^[18] united-atom force field for cellulose and the simple point-charge model^[18] for water, both with bond constraints. Coulomb interactions were truncated at 1 nm with a reaction-field correction (dielectric constant 78.5).^[19]

The hydrophilicity/hydrophobicity at a point *r* was quantified by the local value of the chemical potential of water $\mu_{\text{H}_2\text{O}}(\mathbf{r})$ relative to that of bulk water $\mu_{\text{H}_2\text{O}}(\text{bulk})$. This difference in chemical potential is given by the ratio of the local water density $\rho_{\text{H}_2\text{O}}(\mathbf{r})$ and the bulk density $\rho_{\text{H}_2\text{O}}(\text{bulk})$, Equation (1) ($R = 8.3145 \text{ J mol}^{-1} \text{ K}^{-1}$).

$$\Delta\mu_{\text{H}_2\text{O}}(\mathbf{r}) = \mu_{\text{H}_2\text{O}}(\mathbf{r}) - \mu_{\text{H}_2\text{O}}(\text{bulk}) = -RT \ln \frac{\rho_{\text{H}_2\text{O}}(\mathbf{r})}{\rho_{\text{H}_2\text{O}}(\text{bulk})} \quad (1)$$

A value of $\Delta\mu_{\text{H}_2\text{O}}(\mathbf{r}) < 0$ indicates hydrophilicity and $\Delta\mu_{\text{H}_2\text{O}}(\mathbf{r}) > 0$ hydrophobicity at *r*. Figure 1 shows $\Delta\mu_{\text{H}_2\text{O}}$ as a function of the distance *z* from the cellulose surface, that is,

[*] Priv.-Doz. Dr. F. Müller-Plathe, Dipl.-Chem. O. Biermann
Max-Planck-Institut für Polymerforschung
Ackermannweg 10, 55128 Mainz (Germany)
Fax: (+49) 6131-379-340
E-mail: mplathe@mpip-mainz.mpg.de
Dr. E. Hädicke, Dr. S. Koltzenburg
BASF AG
67056 Ludwigshafen (Germany)

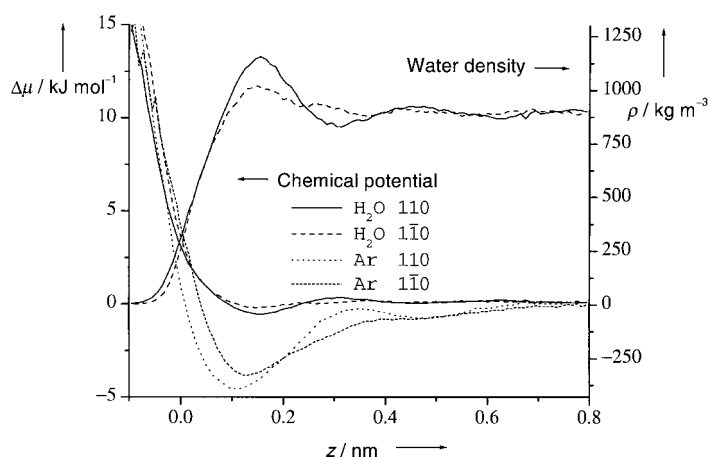


Figure 1. Local chemical potential μ [kJ mol⁻¹] (left scale) of water $\Delta\mu_{\text{H}_2\text{O}}(z)$ and argon $\Delta\mu_{\text{Ar}}(z)$ as a function of the distance z [nm] from the cellulose I β 110 and 11 $\bar{0}$ surfaces, respectively. Also given are the water density profiles [kg m⁻³] (right scale) above both surfaces.

averaged over x and y . The enrichment of water near both surfaces is minute and the basins of negative chemical potential at $z \sim 0.15$ nm are shallow (-0.56 (110), -0.21 kJ mol⁻¹ (11 $\bar{0}$)). Hence, both surfaces are in essence nonhydrophilic. This is also evident in the water-density profile normal to the surface, which lacks the sharp first peak characteristic for hydrophilic surfaces.^[20] The 110 surface has a second, even shallower, chemical potential minimum (at $z \sim 0.47$ nm), which we attribute to its wider lateral spacing between the cellulose chains.

Lipophilicity is not necessarily the opposite of hydrophilicity, but must be similarly quantified by the chemical potential difference of an appropriately chosen “lipophile”. Since our interest is in the adsorption of small lipophilic moieties (present in low concentrations in the water phase) rather than entire molecules, we chose as the lipophile a model argon atom,^[21] which is similar in size and cohesion to a methylene group. Moreover, its size is comparable to that of a water molecule, so probes of similar diameter are used for both hydrophilicity and lipophilicity. Its local excess chemical potential $\mu_{\text{Ar}}^{\text{ex}}(\mathbf{r})$ is obtained by spatially resolved test-particle insertion,^[22] Equation (2), where the angle brackets denote ensemble averaging and $E(\mathbf{r})$ is the change in potential energy on insertion of an argon atom into the cellulose–water system at position \mathbf{r} .

$$\mu_{\text{Ar}}^{\text{ex}}(\mathbf{r}) = -RT \ln(\exp(-E(\mathbf{r})/RT)) \quad (2)$$

The excess chemical potential of argon in bulk water $\mu_{\text{Ar}}^{\text{ex}}(\text{bulk}) = +6.0$ kJ mol⁻¹ (experiment: $\sim +10$ kJ mol⁻¹)^[23] is calculated in a similar way. Figure 1 shows $\Delta\mu_{\text{Ar}}(z) = \mu_{\text{Ar}}^{\text{ex}}(z) - \mu_{\text{Ar}}^{\text{ex}}(\text{bulk})$. Both surfaces exhibit clear minima of -4.5 (110) and -3.8 kJ mol⁻¹ (11 $\bar{0}$). As RT at 333 K equals 2.8 kJ mol⁻¹, both would attract small lipophiles from aqueous solution. More obvious than in the corresponding $\Delta\mu_{\text{H}_2\text{O}}(z)$

curves, the $\Delta\mu_{\text{Ar}}(z)$ curve of 110 has two minima, that for 11 $\bar{0}$ has one. The intervening maximum (at $z \sim 0.32$ nm) of the 110 curve is a shoulder for 11 $\bar{0}$.

Hydrophilicity and lipophilicity can also be resolved laterally to study the distribution of hydrophilic/phobic and lipophilic/phobic spots on the surface. We use a mesh of 0.095×0.102 (110, Figure 2) and 0.095×0.090 nm² (11 $\bar{0}$, Figure 3) resolution in x and y over a layer 0.2 nm thick (z) above the surface. The effect of the crystal structure on hydrophilicity and lipophilicity patterns is clearly visible (Figures 2 and 3), with only some variation due to a small disorder. Note that the atoms shown in the figures are a guide to the eye only, as the surface atoms have substantial positional fluctuations during the course of an MD simulation. In most cases, the lipophilic and hydrophobic areas (both dark red) coincide for both surfaces, the lipophilic areas being somewhat larger. Although surprising at first, this is easily explained, as the exclusion is steric for both water and argon. There is, however, a qualitative difference between the hydrophilic and lipophilic regions: Lipophilic patches (dark blue) are nearly equal in size to the lipophilic ones. In contrast, there are only small hydrophilic spots, as most of the nonhydrophobic surface is “neutral” (green: $\Delta\mu_{\text{H}_2\text{O}} \sim 0$ kJ mol⁻¹) with the same water density as bulk water. The differences between the patterns of the two surfaces are small for both hydrophilicity and lipophilicity.

Local hydrophilicity and lipophilicity are related to the functional groups presented to the water phase. Figure 4 shows hydrophilicity and lipophilicity above a single cellobiose unit on the 110 surface. (The patterns on the 11 $\bar{0}$ surface are qualitatively very similar, therefore they are not shown and only major differences between the two surfaces are mentioned below.) They have been obtained by averaging over all corresponding repeat units and, thus, include static

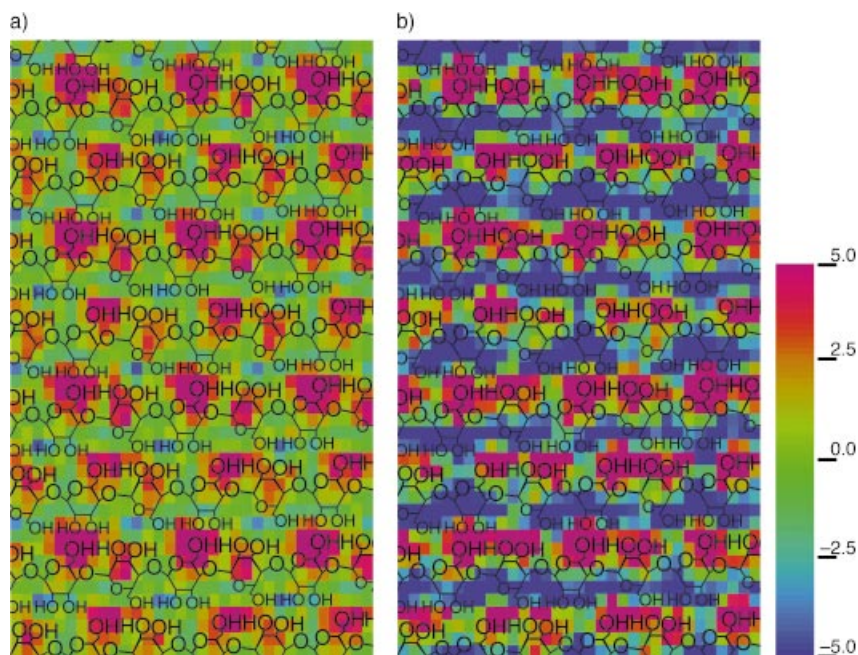


Figure 2. Hydrophilicity and lipophilicity charts of the cellulose I β 110 surface in a layer between $z = 0$ and 0.2 nm. The surface cellulose chains are shown to provide a rough indication of the positions of chemical groups. The lateral grid spacing is approximately 0.1 nm, see text. a) $\Delta\mu_{\text{H}_2\text{O}}(x,y)$ [kJ mol⁻¹]; b) $\Delta\mu_{\text{Ar}}(x,y)$ [kJ mol⁻¹].

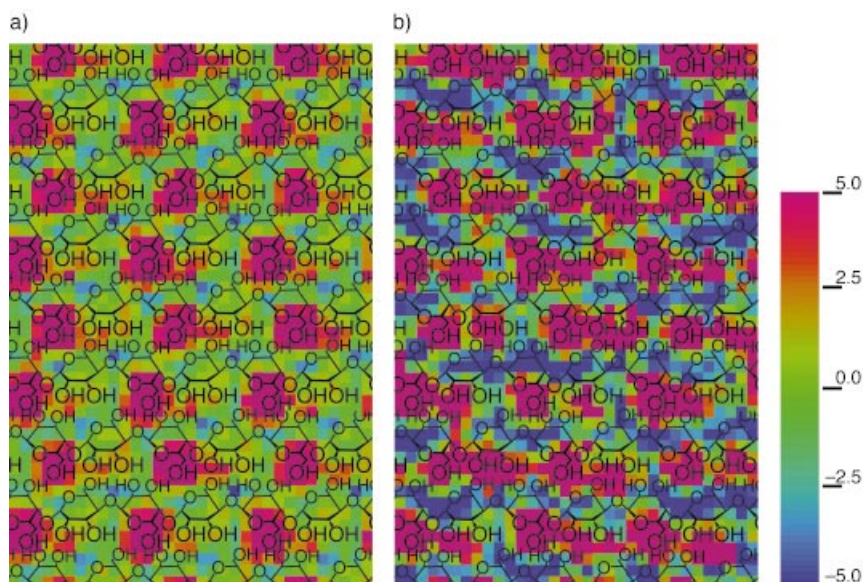


Figure 3. Hydrophilicity and lipophilicity chart of the cellulose $I\beta$ $1\bar{1}0$ surface in a layer between $z = 0$ and 0.2 nm. The plot details are the same as in Figure 2. a) $\Delta\mu_{\text{H}_2\text{O}}(x,y)$ [kJ mol^{-1}]; b) $\Delta\mu_{\text{Ar}}(x,y)$ [kJ mol^{-1}].

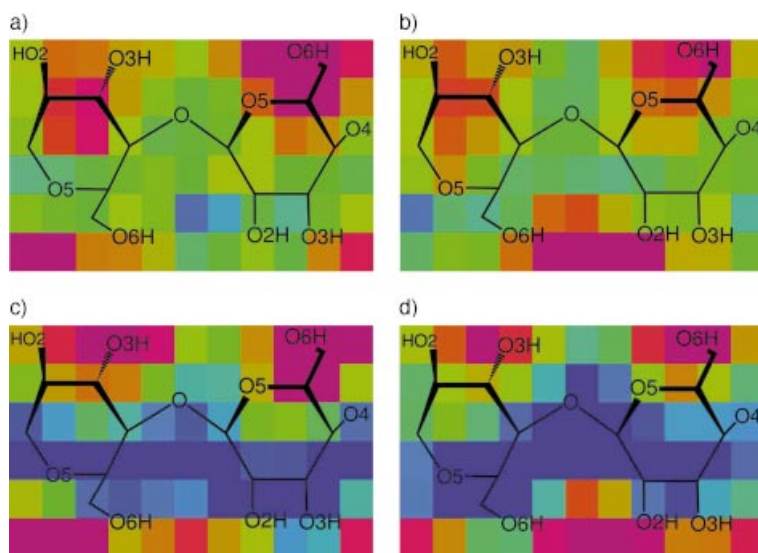


Figure 4. Averaged hydrophilicity $\Delta\mu_{\text{H}_2\text{O}}(x,y)$ [kJ mol^{-1}] and lipophilicity $\Delta\mu_{\text{Ar}}(x,y)$ [kJ mol^{-1}] above a single cellobiose unit on the cellulose $I\beta$ 110 (wide) surface. a) $\Delta\mu_{\text{H}_2\text{O}}(x,y)$ for even-numbered cellulose chains; b) $\Delta\mu_{\text{H}_2\text{O}}(x,y)$ for odd-numbered chains; c) $\Delta\mu_{\text{Ar}}(x,y)$ for even-numbered chains; d) $\Delta\mu_{\text{Ar}}(x,y)$ for odd-numbered chains. The color code is the same as in Figures 2 and 3. Averaging was performed over all 12 crystallographically equivalent cellobiose units of the even or odd chains, respectively, in a layer above the surface between $z = 0$ and 0.2 nm. The structural formulae reflect average atomic positions and are meant as an aid to orientation only.

and dynamic disorder. There are two crystallographically different types of chains, denoted even (Figures 4a and 4c) and odd (Figures 4b and 4d), which have been averaged separately. Even and odd refers to the sequence number of the cellulose chains on the surface counted from the top in Figure 2. For both types of cellulose chains (Figures 4a and 4b), the protruding C6/O6 units and, to a lesser extent, the C2/O2 moieties create hydrophobic areas (high chemical potential towards water). This is due to their space requirements. The effect is slightly more pronounced for the narrow $1\bar{1}0$

surface due to the stronger tilt of the glucose rings. The chain packing in the two surfaces also has an effect on the type of contacts a water molecule has with the surface groups (Table 1). They are obtained by integrating the appropriate partial radial distribution functions (not shown) between water oxygen atoms and different surface groups.^[24] For both surfaces, half of the water contacts are, on average, “hydrophilic” OH groups. On the wider 110 surface, the remaining contacts are equally divided between “hydrophobic” groups and “intermediate” groups. This distribution is shifted from the hydrophobic to the intermediate groups in case of the narrower $1\bar{1}0$ surface.

The lipophobicity (high chemical potential towards argon, dark red) follows qualitatively the hydrophobicity, since it is also mainly due to excluded volume (Figures 4c and 4d). However, the spatial variation of $\Delta\mu_{\text{Ar}}(x,y)$ is larger than that of $\Delta\mu_{\text{H}_2\text{O}}(x,y)$, and there are attractive (dark blue) sites as well. For the 110 surface, they form continuous grooves (Figures 4c and 4d), whereas on the narrow $1\bar{1}0$ surface the attractive patches are not connected, probably due to the lack of space. The lipophilic areas are generally located in depressions on the surface and are lined by hydrophobic atoms such as ether oxygen atoms (O4 and O5) and apolar carbon atoms (C1, C4, and C5). This is also reflected in the surface contacts of argon (Table 1): On the $1\bar{1}0$ surface, the distribution of argon contacts closely resembles that of water contacts, steric accessibility being the criterion for both interactions. In contrast, on the wider 110 surface, the hydrophobic groups are more exposed, and more interactions with them are found.

In summary, both interfaces of cellulose $I\beta$ share common features. Both are stable with respect to surface reconstruction and water penetration, at least on the nanosecond time scale and in the absence of defects. Both show essentially the crystal structure of cellulose $I\beta$, also in the adsorption patterns for water and argon. In

Table 1. Types of surface contacts and their distribution (in percent of all surface contacts) for a water molecule and an argon atom as the prototype lipophile.

Surface groups	H_2O		Ar	
	110	$1\bar{1}0$	110	$1\bar{1}0$
hydrophilic: O2, O3, O6	49.0	51.6	36.8	47.4
intermediate: C2, C3, C6	25.6	29.3	22.9	31.4
hydrophobic: C1, C4, C5, O4, O5	25.4	19.1	40.3	21.2

spite of the presence of OH groups, both surfaces are nonhydrophilic and lipophilic: Water molecules are not attracted to the surface, as they are equally happy in bulk water. On the other hand, the presence of the surface perturbs the water structure sufficiently to create free volume, in which an argon atom (and, hence, a small lipophilic moiety of an organic adsorbent) can dissolve more easily than in the denser bulk water. The wider spacing of cellulose chains allows the 110 surface to expose more of the hydrophobic grooves where lipophilic adsorption takes place. In contrast, the protruding OH groups are less affected by chain packing, so the behavior towards water is similar for both surfaces.

Received: June 8, 2001 [Z17256]

Electronic Semiconductor–Support Interaction—A Novel Effect in Semiconductor Photocatalysis**

Harald Weiß, Asuncion Fernandez, and Horst Kisch*

*Dedicated to Professor Yasuo Wakatsuki
on the occasion of his 60th birthday*

The growing field of semiconductor photocatalysis has moved from basic research to practical applications. Typical examples are the detoxification of air and water^[1] and novel organic syntheses^[2] photocatalyzed by titania and cadmium sulfide. The photonic efficiency of these transformations largely depends on the ratio of the rate of interfacial electron transfer (IFET) to the rate of recombination of the photo-generated electron-hole pair. It is generally assumed that only substrates adsorbed at the semiconductor surface can participate in the IFET. Therefore in many cases the reaction rate increases when substrate adsorption is improved. A better adsorption was also invoked to rationalize the higher detoxification rates induced by supporting semiconductors like titania onto silica or alumina.^[3]

During our work on addition reactions photocatalyzed by semiconductors (semiconductor photocatalysis type B) we observed that precipitation of cadmium sulfide onto silica afforded a much better photocatalyst than the unsupported material. Herein we report on experimental evidence that this enhanced photocatalytic activity does not stem from improved adsorption but rather from an electronic semiconductor–support interaction (SEMSI), which alters the bandgap energy and flatband potential. Whereas electronic catalyst–support interactions are well documented in thermal heterogeneous catalysis, they have been unknown in the field of semiconductor photocatalysis.


Thus, whereas the reaction between cyclopentene (RH) and the Schiff base **1** (Scheme 1)^[2d,e] is quite slow in the presence of CdS it becomes about 10 times faster when silica covered with 50% CdS (CdS-50/SiO₂) is used as the photocatalyst. According to the proposed mechanism, the intermediate aminobenzyl and allyl radicals are formed through proton-coupled IFET reactions of the substrates with reactive electrons and holes (e⁻, h⁺). Their C–C hetero- and homocoupling lead to **2** and **3** as the major and by-product, respectively.^[2d,e]

- [1] S. Imam, R. V. Green, B. R. Zaidi, *Biopolymers—Utilizing Nature's Advanced Materials*, American Chemical Society, Washington, DC, **1998**.
- [2] J. C. Roberts, *The Chemistry of Paper*, Royal Society of Chemistry, Cambridge, **1996**.
- [3] T. Heinze, U. Erler, I. Nehls, D. Klemm, *Angew. Makromol. Chem.* **1994**, 215, 93–106; A. Baar, W. M. Kulicke, K. Szablikowski, R. Kiesewetter, *Macromol. Chem. Phys.* **1994**, 195, 1483–1492.
- [4] F. Müller-Plathe, H. Schmitz, R. Faller, *Prog. Theor. Phys. Suppl.* **2000**, 138, 311–319.
- [5] A. A. Baker, W. Helbert, J. Sugiyama, M. J. Miles, *J. Struct. Biol.* **1997**, 119, 129–138.
- [6] A. A. Baker, W. Helbert, J. Sugiyama, M. J. Miles, *Appl. Phys. A* **1998**, 66, S559–S563.
- [7] A. A. Baker, W. Helbert, J. Sugiyama, M. J. Miles, *Biophys. J.* **2000**, 79, 1139–1145.
- [8] A. Aabloo, A. D. French, *Macromol. Theory Simul.* **1994**, 3, 185–191.
- [9] S. Reiling, J. Brickmann, *Macromol. Theory Simul.* **1995**, 4, 725–741.
- [10] S. K. Cousins, R. M. Brown, Jr., *Polymer* **1995**, 36, 3885–3888.
- [11] A. P. Heiner, J. Sugiyama, O. Teleman, *Carbohydr. Res.* **1995**, 273, 207–232.
- [12] B. J. Hardy, A. Sarko, *Polymer* **1996**, 37, 1833–1839.
- [13] A. P. Heiner, O. Teleman, *Langmuir* **1997**, 13, 511–518.
- [14] A. P. Heiner, L. Kuutti, O. Teleman, *Carbohydr. Res.* **1998**, 306, 205–220.
- [15] J. Ganster, H.-P. Fink in *Polymer Handbook* (Eds.: J. Brandrup, E. H. Immergut, E. A. Grulke), Wiley, New York, NY, **1999**.
- [16] J. Sugiyama, R. Vuong, H. Chanzy, *Macromolecules* **1991**, 24, 4168–4175.
- [17] H. J. C. Berendsen, J. P. M. Postma, W. F. van Gunsteren, A. DiNola, J. R. Haak, *J. Chem. Phys.* **1984**, 81, 3684–3690.
- [18] W. F. van Gunsteren, S. R. Billeter, A. A. Eising, P. H. Hünenberger, P. Krüger, A. E. Mark, W. R. P. Scott, I. G. Tironi, *Biomolecular Simulation: The GROMOS96 Manual and User Guide*, vdf, Zurich, **1996**.
- [19] F. Müller-Plathe, *Comput. Phys. Commun.* **1993**, 78, 77–94.
- [20] J. R. Grigera, S. G. Kalko, J. Fischbarg, *Langmuir* **1996**, 12, 154–158.
- [21] B. Guillot, Y. Guissani, *J. Chem. Phys.* **1993**, 99, 8075–8094.
- [22] F. Müller-Plathe, *J. Chem. Phys.* **1995**, 103, 4346–4351.
- [23] *Handbook of Chemistry and Physics*, 74th ed. (Ed.: D. R. Lide), CRC Press, Boca Raton, FL, **1993**.
- [24] F. Müller-Plathe, W. F. van Gunsteren, *Polymer* **1997**, 38, 2259–2268.

[*] Prof. Dr. H. Kisch, Dipl.-Chem. H. Weiß
Institut für Anorganische Chemie der Universität Erlangen-Nürnberg
Egerlandstrasse 1, 91058 Erlangen (Germany)
Fax: (+49) 9131-8527363
E-mail: kisch@chemie.uni-erlangen.de

Dr. A. Fernandez
Instituto de Ciencia de Materiales de Sevilla
Dpto. Química Inorgánica
Centro de Investigaciones Científicas Isla de la Cartuja
Avda. Américo Vespucio s/n, 41092 Sevilla (Spain)

[**] This work was supported by the Volkswagen-Stiftung, the Deutsche Forschungsgemeinschaft, and Fonds der Chemischen Industrie. Helpful discussions with D. Meissner are gratefully acknowledged.

 Supporting information for this article is available on the WWW under <http://www.angewandte.com> or from the author.